EUROPEAN ORGANIZATION FOR NUCLEAR RESEARCH

CERN-EP/90-62
11 May 1990

A LARGE-AREA TRANSITION RADIATION DETECTOR

G.D. Barr, R. Carosi, L. Gatignon, V. Gibson, R. Hagelberg,
J. van der Lans, H.N. Nelson and H. Wahl
CERN, Geneva, Switzerland

D.J. Candlin and K.J. Peach
Physics Department, University of Edinburgh, UK

H. Blümer, R. Heinz, K. Kleinknecht, P. Mayer, B. Panzer,
B.Renk and H. Rohrer
Institut für Physik, Universität Mainz, Fed. Rep. Germany[a]

E. Augé, D. Fournier, I. Harrus, P. Heusse,
L. Iconomidou-Fayard and A.C. Schaffer
Laboratoire de l'Accélérateur Linéaire, Université de Paris-Sud, Orsay, France[b]

L. Bertanza, A. Bigi, P. Calafiura, M. Calvetti[1], C. Cerri, R. Fantechi, G. Gargani,
I. Mannelli[2] and G.M. Pierazzini
Dipartimento di Fisica e Sezione INFN, Pisa, Italy

C. Becker[3], H. Burkhardt, M. Holder, A. Kreutz, R. Ossa[4], M. Rost and H.G. Sander[5]
Fachbereich Physik, Universität Siegen, Fed. Rep. Germany[c]

(Submitted to Nuclear Instruments and Methods in Physics Research)

---

1) Present address: Dipartimento di Fisica e Sezione INFN, Perugia, Italy.
2) Present address: Scuola Normale Superiore, Pisa, Italy.
3) Present address: DVFLR, Cologne, Fed. Rep. Germany.
4) Present address: SLAC, Stanford, Calif., USA.
5) Present address: Institut für Physik, Universität Mainz, Fed. Rep. Germany.

a) Funded by the German Federal Minister for Research and Technology (BMFT) under contract 054MZ18.
b) Funded by the Institut National de Physique Nucléaire et Physique des Particules (IN2P3), France.
c) Funded by the German Federal Minister for Research and Technology (BMFT) under contract 054Si74.

ABSTRACT

The construction and the operation of a large-area transition radiation detector (TRD) for the NA31 experiment at CERN are described. The TRD incorporates several novel features for stabilizing the detector response. The density of the gas mixture (xenon + helium + methane) in the detection chambers is matched to the carbon dioxide gas in the surrounding radiators by tuning the helium concentration to avoid a hydrostatic pressure difference, which would deform the chamber walls. The chamber pressure is continuously regulated by computer control to maintain it to within 1 μbar of the radiator pressure. The gas gain of each of the four chambers is regulated to better than 0.2% by changing the high voltage under computer control, using the pulse-height spectra of 16 cadmium-109 sources mounted on the chambers. The results of performance studies are described. The detector has a pion efficiency of 98.7% with an electron rejection of a factor of 10.

1. INTRODUCTION

The NA31 experiment at CERN has reported evidence for direct CP violation in the two-pion decay modes of the neutral kaon system [1]. Direct CP violation is studied by looking for a small difference in the ratio of the two-charged-pion decay rate to the two-neutral-pion decay rate in beams of short- and long-lived kaons. An important part of the analysis is to subtract background from the $K_L \to \pi^+\pi^-$ decay mode. The final sample reported in ref. [1] contained 0.7% background, of which 70% is estimated to be from $K_L \to \pi e \nu$ (K_{e3}). In order to reduce the systematic error on the background subtraction, a transition radiation detector (TRD) was added for the data collection periods of 1988 and 1989 to reduce the K_{e3} background by another order of magnitude.

2. DETECTOR OPTIMIZATION

The NA31 detector configuration for the period up to the end of the 1987 run is described in an earlier article [2]. The TRD was added directly behind the second of the two drift chambers, in front of the aluminium end-cap that precedes the liquid-argon calorimeter. This has necessitated a slight rearrangement of some of the existing detectors. A hole in the centre of the TRD accommodates the beam pipe.

The detector (fig. 1) consists of four stacks of thin-foil polypropylene radiators, which cause highly relativistic particles, such as electrons, to radiate X-rays in the 10 keV energy range. A proportional wire chamber, immediately downstream from each radiator stack, is filled with a mixture of xenon, helium, and methane. The xenon has a high absorption cross-section for the X-rays, which are then detected by an enhancement of the pulse height on the wires.

A detailed study was made in order to optimize the detector parameters so as to maximize the electron–pion separation in the energy range of interest (20–90 GeV) [3]. The design was constrained by the space available longitudinally and by the need to minimize the amount of matter through which the particles must pass. The final detector specification is shown in table 1. As a consequence of the requirement that the amount of material in the particle path be minimized, the wire chamber walls were made of flexible Mylar sheets. To maintain the flatness of the Mylar sheets, the density of the wire chamber gas must be the same as that gas in the adjacent radiators. Use of the heavy gas CO_2 in the radiators, instead of air, allows a higher concentration of xenon in the chambers, thus increasing the number of X-rays converted in the chambers, for the same thickness of the charge collection region and maximum drift time.

3. RADIATOR CONSTRUCTION

Each polypropylene foil*) is in the form of a single octagonal sheet. A 0.7 m long aluminium strip is attached to each of the eight edges with double-sided adhesive tape. The total thickness of the strip and tape define the radiator foil separation to be 600 μm. The radiators are suspended in gas-tight frames by springs, which fasten onto tie rods passing through the strips on the foils. The springs hold the radiators under tension in order to keep them flat.

One of the difficulties in constructing such a radiator is that electrostatic forces make the foils stick to each other, which spoils the desired uniform spacing. To overcome this problem, each foil is thermally deformed into a waffle pattern in order to maintain the spacing locally under the tension of the springs. The foils are deformed along a square (3 cm × 3 cm) grid. Consecutive foils have their pattern shifted by (1/2 + 1/32) of a pitch so as to avoid accumulation of the indentations. A semiautomatic machine for producing the indented sheets was designed, built, and operated at

*) 2400 mm wide polypropylene, type 19MB200, from Mobil Plastiques, Belgium.

Orsay. The indentations are made using a steel plate into which wires of diameter 400 μm are woven to form the grid. The fabrication process is as follows.

The steel plate is heated to 65 °C and a sheet of polypropylene is laid across it. The sheet is kept in place by vacuum suction applied through holes in the plate. An octagonal frame on wheels, which has the taped strips attached by suction, is lowered onto the polypropylene. A set of infrared heaters (total power 50 kW) is suspended about 20 cm above the foil and activated for a short time (less than a minute) until the temperature reaches 110 °C. When the plate has cooled to 55 °C, the vacuum is replaced by a small amount of compressed air in order to lift the foil from the surface of the plate. The frame is then raised, and transports the foil to an adjacent stack where the previously made foils are kept on the tie rods. The central hole is cut using a hot wire before dropping the sheet onto the stack. In full production, this cycle takes about 10 minutes per foil.

4. WIRE CHAMBER CONSTRUCTION

A proportional wire chamber is situated immediately behind each of the radiator assemblies. The wire chambers follow the design of the drift chambers [2] used in the experiment. The 218 (30 μm) gold-plated tungsten anode wires in each chamber are strung at a tension of 1.3 N on a Stesalit frame, with a pitch of 1.2 cm. The wires are horizontal in the first and third chambers and vertical in the other two. The anode plane in each chamber is sandwiched between two 75 μm Mylar foil cathodes, which are stretched over Stesalit frames to a tension of 12 N/cm and coated with graphite. The anode–cathode gap is 2.5 cm. A central hole in the chambers and radiators accommodates the beam pipe. The radiators and chambers are shown in detail in figs. 2a and 2b.

5. GAS PRESSURE REGULATION AND PURIFICATION SYSTEM

The TRD chambers and radiators are filled with gas at slightly above atmospheric pressure. The radiators are filled with CO_2 by a simple purge system. The chamber is filled with a mixture of xenon (30%) + helium (55%) + methane (15%), which has the same density as the CO_2 in the radiators. The gas is circulated with a flow rate of 2.5 l/min in a closed-loop system (fig. 3). The purification system comprises a catalytic burner and a molecular sieve. The catalytic burner converts O_2 and CH_4 to H_2O and CO_2 by passing the chamber gas over a palladium catalyser at 450 °C. The molecular sieve absorbs the reaction products. The gas system contains two molecular sieves, so that one can be regenerated while the other is in use.

A second function of the gas system is to regulate the pressure in the chambers to 1 μbar with respect to the radiator pressure. The gas volumes are interconnected at the top and bottom of the four chambers and at half height, and the pressure of all four chambers is regulated as a single unit. The inlet flow rate is constant, and the chamber pressure is controlled by adjusting the outlet flow with a valve. The differential pressure between the chambers and the radiators is measured at half height by a pressure transducer*). This value is used by a microprocessor to compute a new valve position every 50 s. Figure 4 shows the variation of the differential pressure over a two-hour period. The gas system contains a 100 l reserve tank which is used to store the excess gas used to compensate changes in the atmospheric pressure.

Two more pressure transducers**) measure the differential pressure at the top and bottom of the chambers and monitor the hydrostatic pressure difference. Since helium is lost preferentially, a pressure difference gradually builds up (1 μbar per 3 l of helium). To correct for this loss, the microprocessor uses the data from these transducers to inject helium automatically every three hours. About 20 l of helium are injected each day.

---

*) MKS Baratron 220 BD.

**) MKS Baratron 223 BD.

6. ELECTRONIC READOUT SYSTEM

Two adjacent wires (three at the edges) are connected and read out with one electronic channel, such that there are 96 channels per chamber. The preamplifier and readout electronics are similar to those used for the NA31 liquid-argon calorimeter [2]. The charge preamplifiers are mounted directly on the chamber support, outside the gas enclosure, and have a gain of 2 mV/fC. They have a decay-time constant of 3.6 μs. The preamplifier drives a 30 m long, twisted-pair cable to the control room, where the signals are processed by sample and hold channels that sample the voltage at three points in time, separated by 2 μs (fig. 5). The quantity $V = 2Q_B - (Q_A + Q_C)$ is digitized. A small correction is made to the above formula to allow for exponential decay. The digitization is done with 12-bit ADCs. A minimum-ionizing particle registers around 300 counts. The electronic noise is about 2 ADC counts—thus completely negligible. The amount of data is reduced by recording only the pulse heights of channels with more than 40 counts and those of their nearest neighbours.

7. GAIN STABILIZATION

An important feature of this detector is the gain-stabilizing control system, which is used to monitor the gain and keep it constant. Four ^{109}Cd sources are installed on each chamber. A computer is used to read and analyse source events and to accumulate histograms. The peak position of the source is kept constant by adjusting the high voltage on the cathodes. This corrects for gain variations caused by pressure, temperature, and changes in the gas composition. The spatial gain variations are also monitored by comparing the peaks from the different sources.

A block diagram of the control system is shown in fig. 6. The signals from 16 wires, which are directly illuminated by each source, are tapped off from the preamplifier cards. The trigger is generated from threshold comparators during the 12 s outside the 2.5 s burst from the Super Proton Synchrotron (SPS). The raw event rate collected by the data acquisition is 4 kHz. A high-voltage correction is made approximately every 6 minutes, when 10^5 events have been recorded from each chamber. The high voltage is controlled separately for each chamber through a DAC. The DAC has a ± 50 V range of control in 0.1 V steps, which is added to an offset that maintains a negative voltage of typically 2.7 kV on the cathodes. During operation, the DAC value changes by one or two steps per correction.

A typical source histogram is shown in fig. 7. Figure 8 shows the variation in the mean gain as a function of time over a period of about 10 hours. Each point corresponds to one correction. The r.m.s. gain variation σ_{gain} is better than 0.2%. Figure 9 shows σ_{gain} as a function of the number of events N_{ch} recorded per chamber. At low N_{ch}, the σ_{gain} is limited by statistics, and at N_{ch} above 100,000, slow variations in the system dominate. During normal running conditions, external pressure variations, caused by the regulation of the helium tank [2], limit σ_{gain} to 0.2%. For a part of the running period, data were acquired from within the SPS burst. These data have been used to show that the gain variation between in-burst and out-of-burst conditions is less than 0.2% [4].

The homogeneity of the gas gain of the chambers was measured using pions from $K_S \rightarrow \pi^+\pi^-$ decays during normal data taking. A systematic dependence on the radial position of the pion impact in the chamber, characterized by a roughly linear 10% decrease between centre and outer border, is observed. This is believed to be caused by a slight bowing of the Mylar cathodes due to a pressure difference offset.

8. PION-ELECTRON SEPARATION

Off line, the TRD signals associated with each charged track are reconstructed first by searching for clusters (in each of the four TRD chambers) and then by selecting the cluster closest to the track trajectory as measured by the drift chambers. The pulse-height distributions from electrons (from K_{e3}

decays) and pions (from $K_S \to \pi^+\pi^-$) are shown in fig. 10. Figure 11 shows the electron pulse-height distribution compared with a Monte Carlo calculation. The Monte Carlo represents the data well, including the rise in the distribution at low pulse height and the shoulder corresponding to electrons where no transition radiation photons are captured in the gas.

The probability of observing one or more extra clusters, besides those associated with the particle tracks, was found to be 35% in $K_S \to \pi^+\pi^-$ events. The extra hits in different chambers have no apparent spatial correlation, their distribution is essentially uniform, and they have a pulse height below that of a minimum-ionizing particle (fig. 12). By studying the pulses in events triggered randomly within the SPS burst, where the probability of finding a hit is much smaller (2% for energies above 5 keV), it has been shown that these pulses are related to the event. One possible explanation is that they are Compton back-scattered photons from the particle showers in the calorimeters downstream from the TRD.

Two methods of combining the pulse heights from the four chambers for each track have been studied.

i) The truncated mean T, i.e. the mean of the lowest three pulse heights in the four chambers. Omission of the highest pulse height reduces the possibility of mistaking a pion, where there is a delta-ray emission, for an electron. The distributions of T for electrons, pions, and muons (from a test beam) are shown in fig. 13. The high-T tail of 1% in the pion data, which is absent in the muon data, is compatible with strong interactions of the pions in the radiator material.

ii) The likelihood ratio

$$L = \prod_{i=1,4} \frac{P_e^i(E)}{P_\pi^i(E)} \quad ,$$

where $P_e^i\,dE$ ($P_\pi^i\,dE$) is the probability that the measured pulse height E in chamber i in an interval dE around E is due to an electron (pion). The distributions $P_e(E)$ and $P_\pi(E)$ are the normalized pulse-height distributions shown in fig. 10. The distributions of log L for electrons and pions is shown in fig. 14.

The pion–electron separation is shown in fig. 15 for various cuts in the variables T and L corresponding to the two methods described above. The likelihood method is slightly better than the truncated mean method. At a cut that rejects 90% of electrons, the loss of pions, which is due to misidentification using the truncated mean and maximum likelihood methods, is 1.7% and 1.3%, respectively.

If the detector were to be used in an experiment to search for an electron signal with pions as background, the rejection power would be a factor of 70 for 90% acceptance to electrons.

Acknowledgements

The success of this project, which was carried out within a very short time-scale, is a tribute to the skills and dedication of many people. We would like to thank in particular F. Berny, J. Brugnon, J.P. Coulon, M. Dialinas, J. Escalera, R. Gläser, A. Krieg, G. Laverrière, P. Le Cossec, J.P. Marolleau, E. Plaige, D. Richard, J.P. Richer and L. Zaccarelli.

REFERENCES

[1] H. Burkhardt et al., Phys. Lett. **206B** (1988) 169.

[2] H. Burkhardt et al., Nucl. Instrum. Methods **A268** (1988) 116.

[3] CERN/SPSC/87-48, SPSC/P174 Add. 4 (1987).

[4] G.D. Barr et al., IEEE Trans. Nucl. Sci. **36** (1989) 66.

Table 1

Transition radiation detector parameters

Number of radiator stacks and chambers	: 4
Thickness of charge collection region per chamber	: 5 cm
Foil thickness	: 19 μm
Foil separation distance	: 600 μm
Number of foils per stack	: 350
Radiator gas	: CO_2
Chamber gas (density matched to radiator gas)	: Xe/He/CH_4
Octagonal active zone with a 120 cm inscribed circle radius	

Figure captions

Fig. 1 TRD radiator and wire chamber construction.
Fig. 2 a) Schematic of TRD radiators and chambers; b) detail of chamber/radiator mounting.
Fig. 3 Schematic of the closed-loop gas system with regulated analogue valves in the inlet and outlet of the chambers.
Fig. 4 Pressure between chamber and radiator as a function of time.
Fig. 5 Pulse shape with three-point sampling in the readout electronic system.
Fig. 6 Block diagram of the gain control system.
Fig. 7 Monitor channel pulse-height distribution, out of burst, showing the peak from the ^{109}Cd source.
Fig. 8 Variation in the mean chamber gain measured from the four sources in each of the four chambers.
Fig. 9 The r.m.s. gain variation as a function of the number of events used to determine the correction.
Fig. 10 Pulse-height distribution for pions and electrons in one chamber.
Fig. 11 Comparison of the observed pulse-height spectrum of electrons in one chamber with Monte Carlo simulation.
Fig. 12 Pulse-height distribution of hits on and far away from tracks in $K_S \rightarrow \pi^+ \pi^-$ decays.
Fig. 13 Truncated mean pulse-height distributions for a) pions, b) muons and c) electrons (units are arbitrary).
Fig. 14 Likelihood distributions for pions and electrons.
Fig. 15 Electron-pion separation curves for the two methods of data analysis.

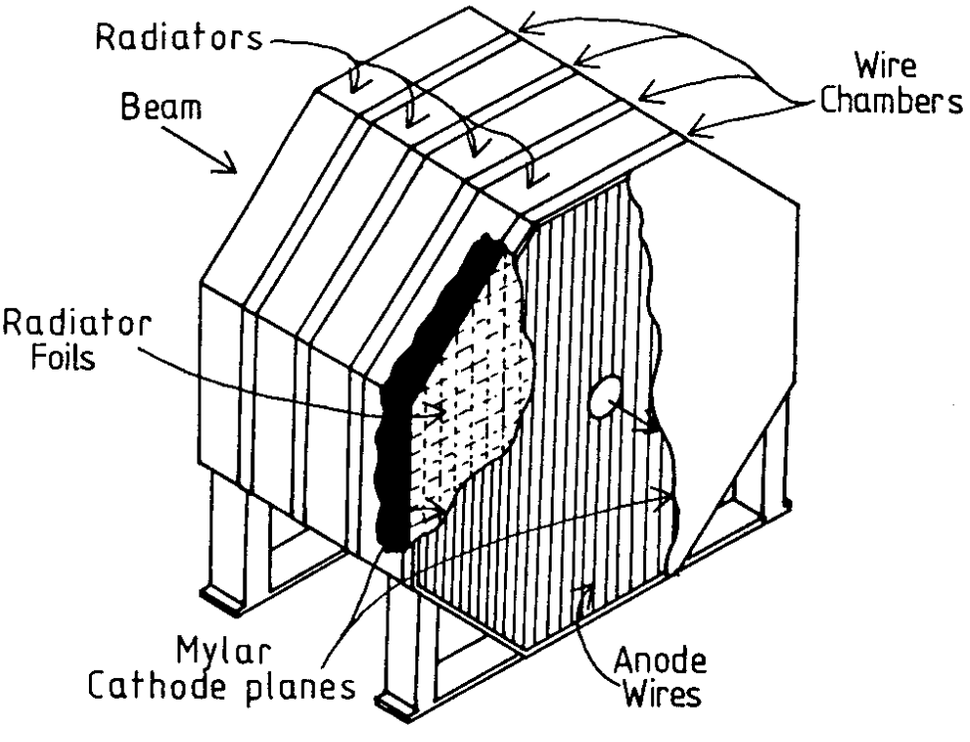

Fig. 1

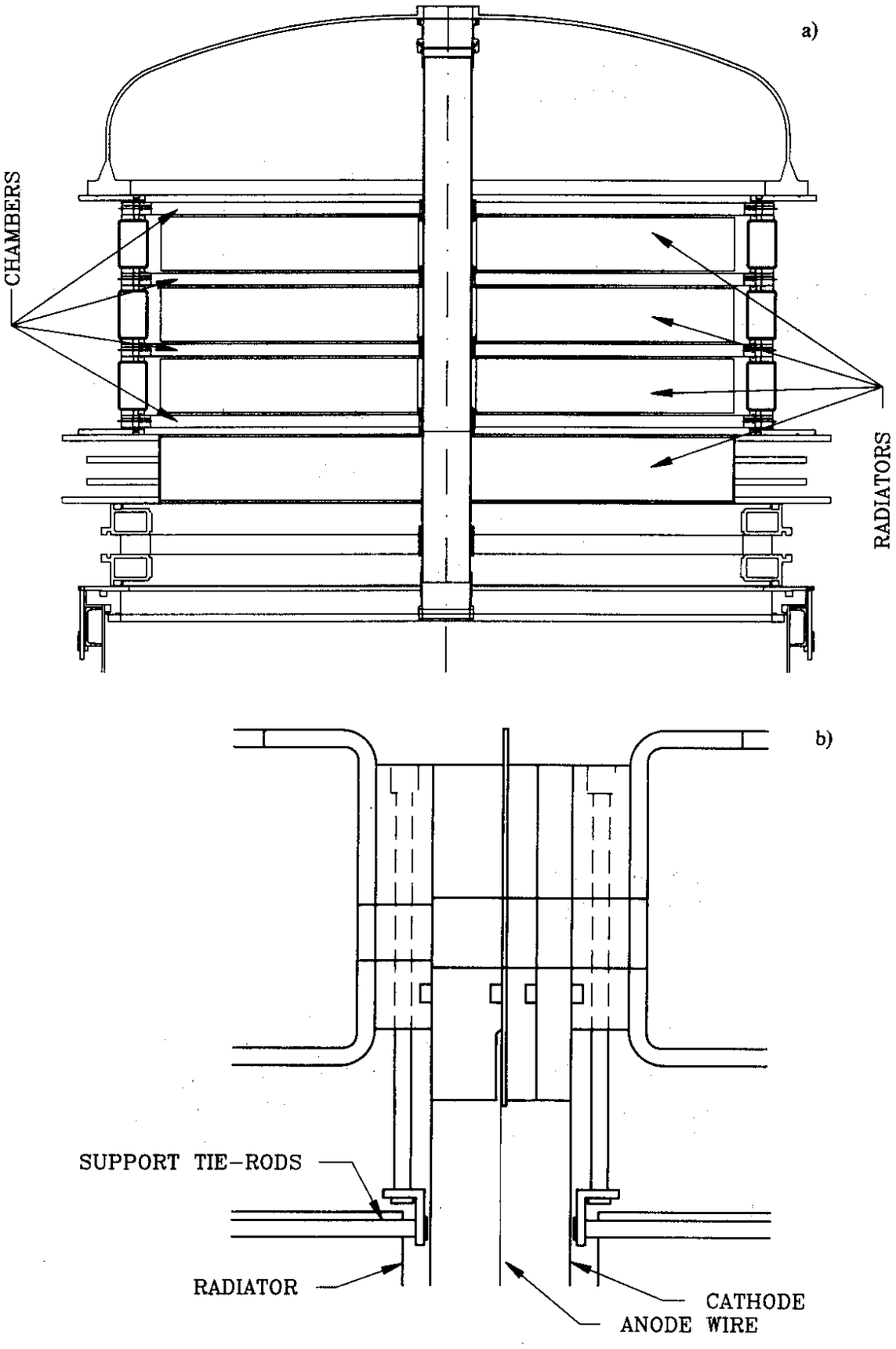
a)
CHAMBERS
RADIATORS
b)
SUPPORT TIE-RODS
RADIATOR
CATHODE
ANODE WIRE

Fig. 2

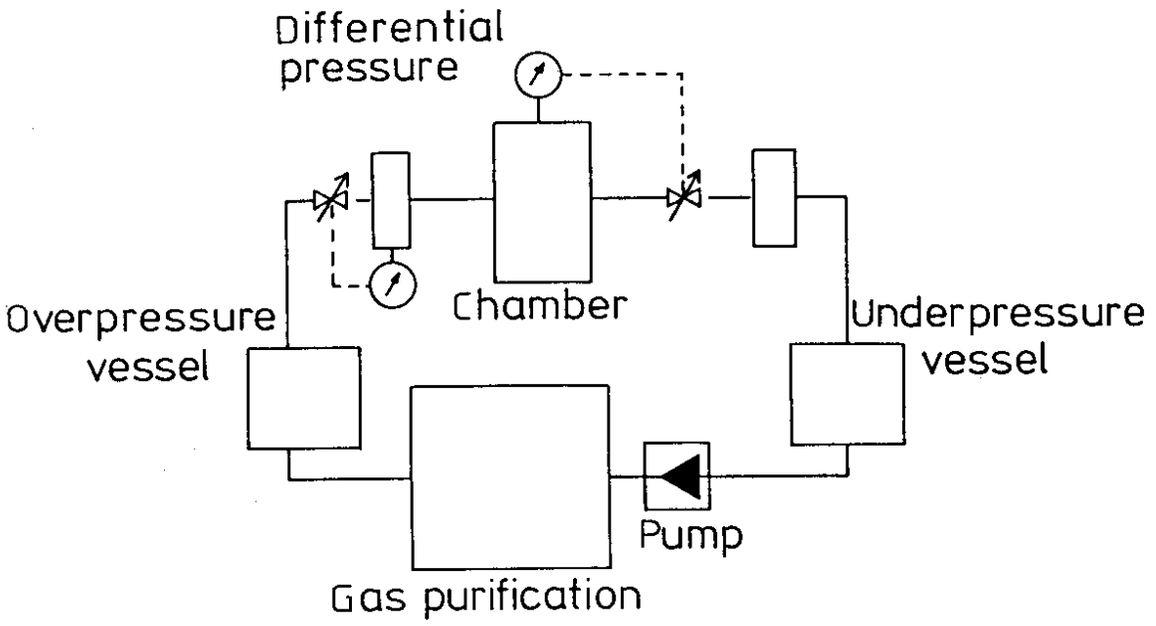
Differential
pressure
Chamber
Overpressure
vessel
Underpressure
vessel
Pump
Gas purification

Fig. 3

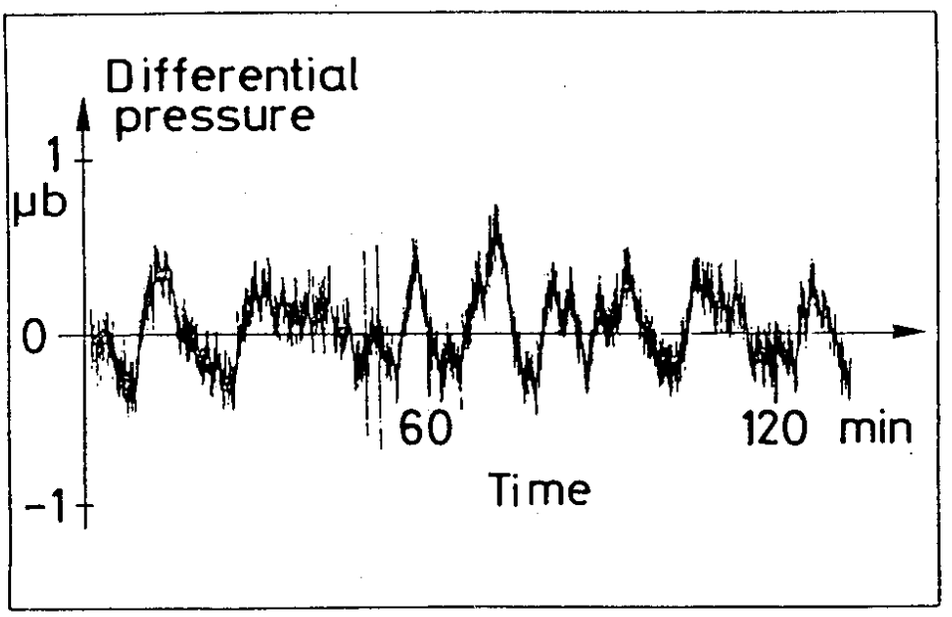
Differential
pressure
1
μb
0
-1
60
120 min
Time

Fig. 4

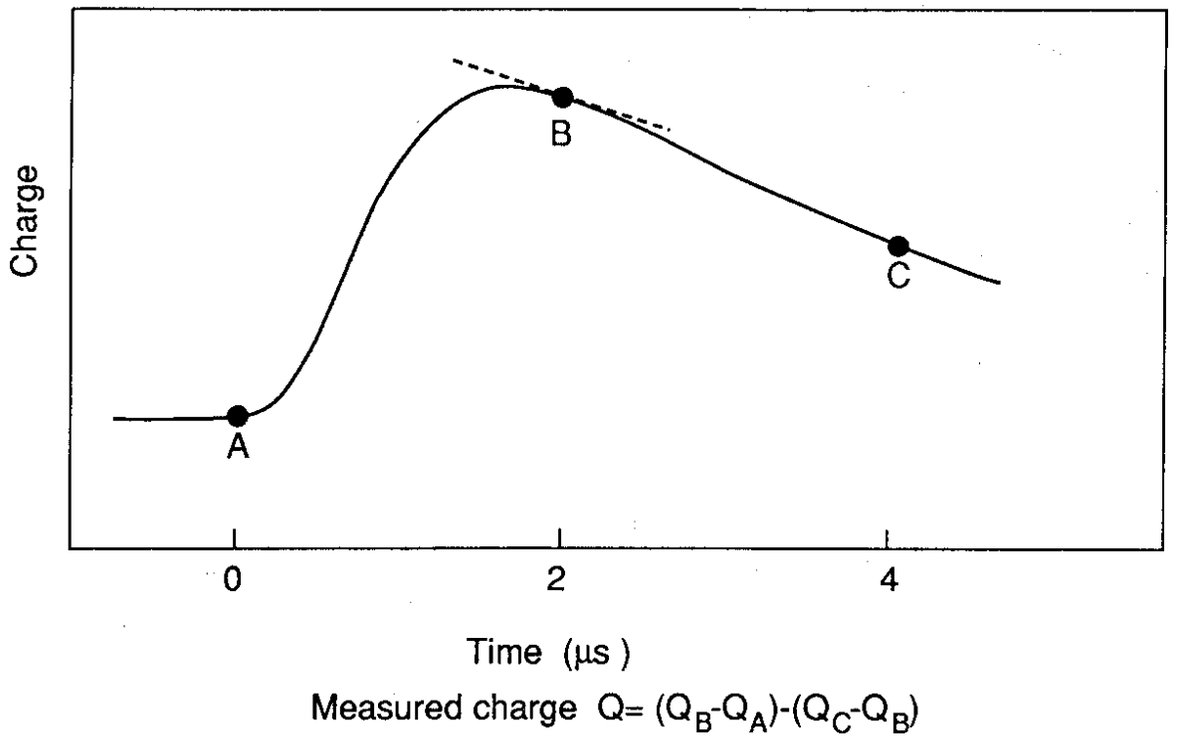
Charge
A
B
C
0
2
4
Time (μs)
Measured charge Q= (Q_B-Q_A)-(Q_C-Q_B)

Fig. 5

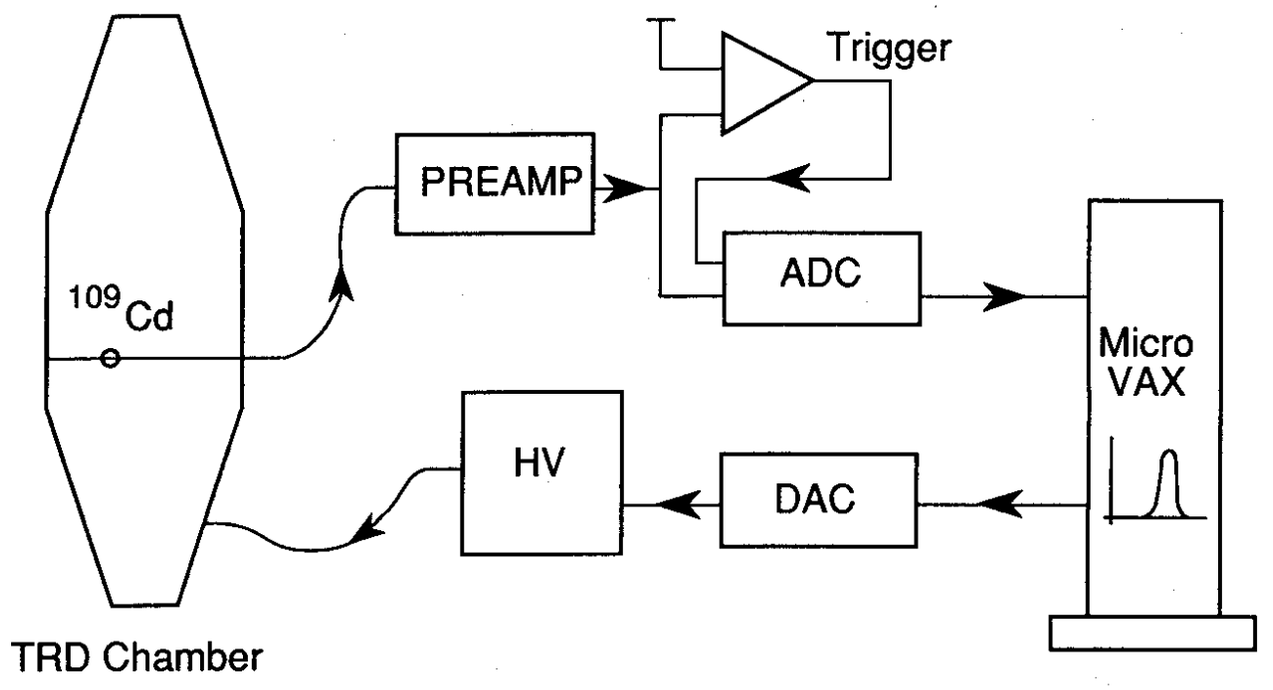
Trigger
PREAMP
ADC
109Cd
Micro VAX
HV
DAC
TRD Chamber

Fig. 6

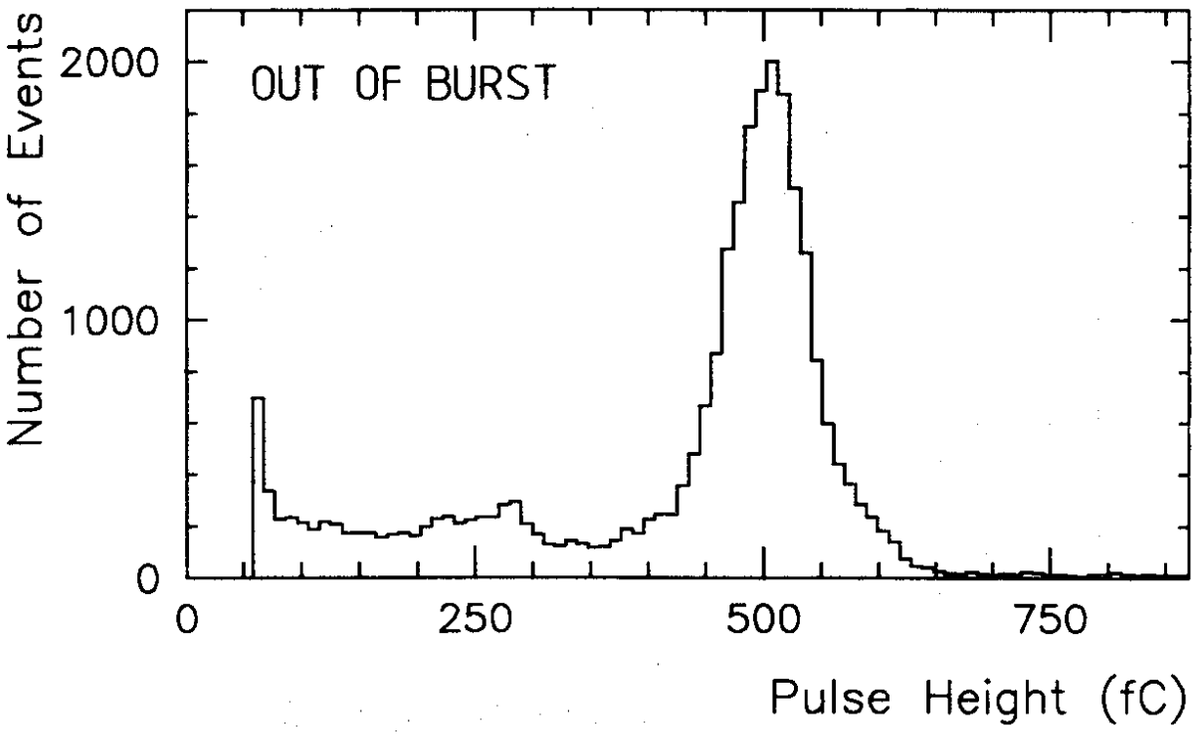
OUT OF BURST
Number of Events
2000
1000
0
0
250
500
750
Pulse Height (fC)

Fig. 7

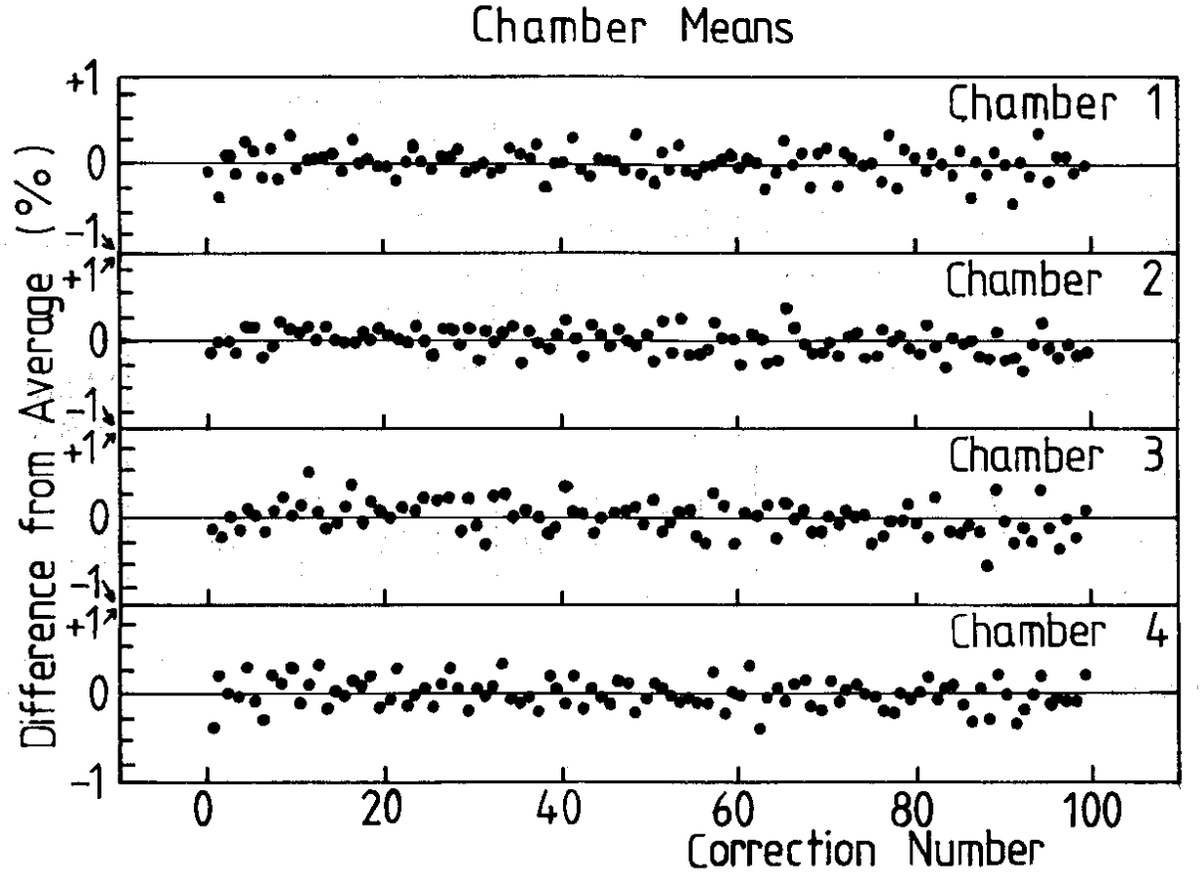
Chamber Means
Chamber 1
Chamber 2
Chamber 3
Chamber 4
Difference from Average (%)
+1
0
-1
0
20
40
60
80
100
Correction Number

Fig. 8

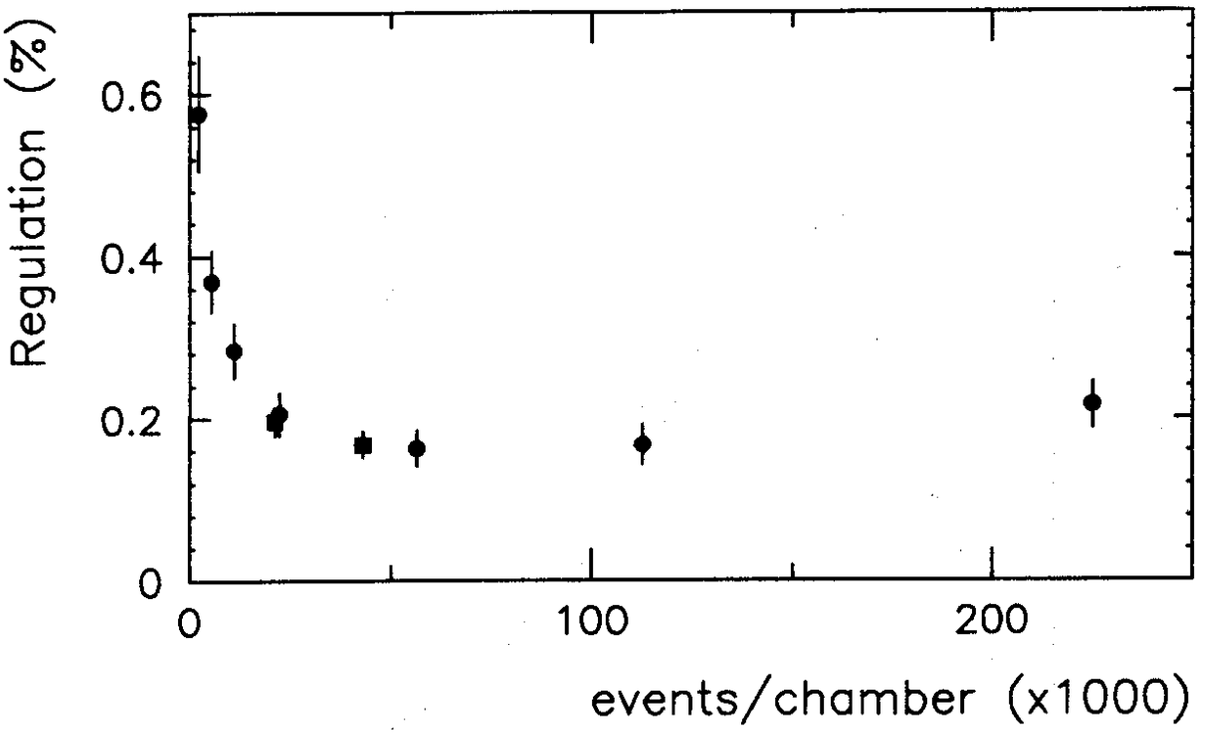
Regulation (%)
0.6
0.4
0.2
0
0
100
200
events/chamber (x1000)

Fig. 9

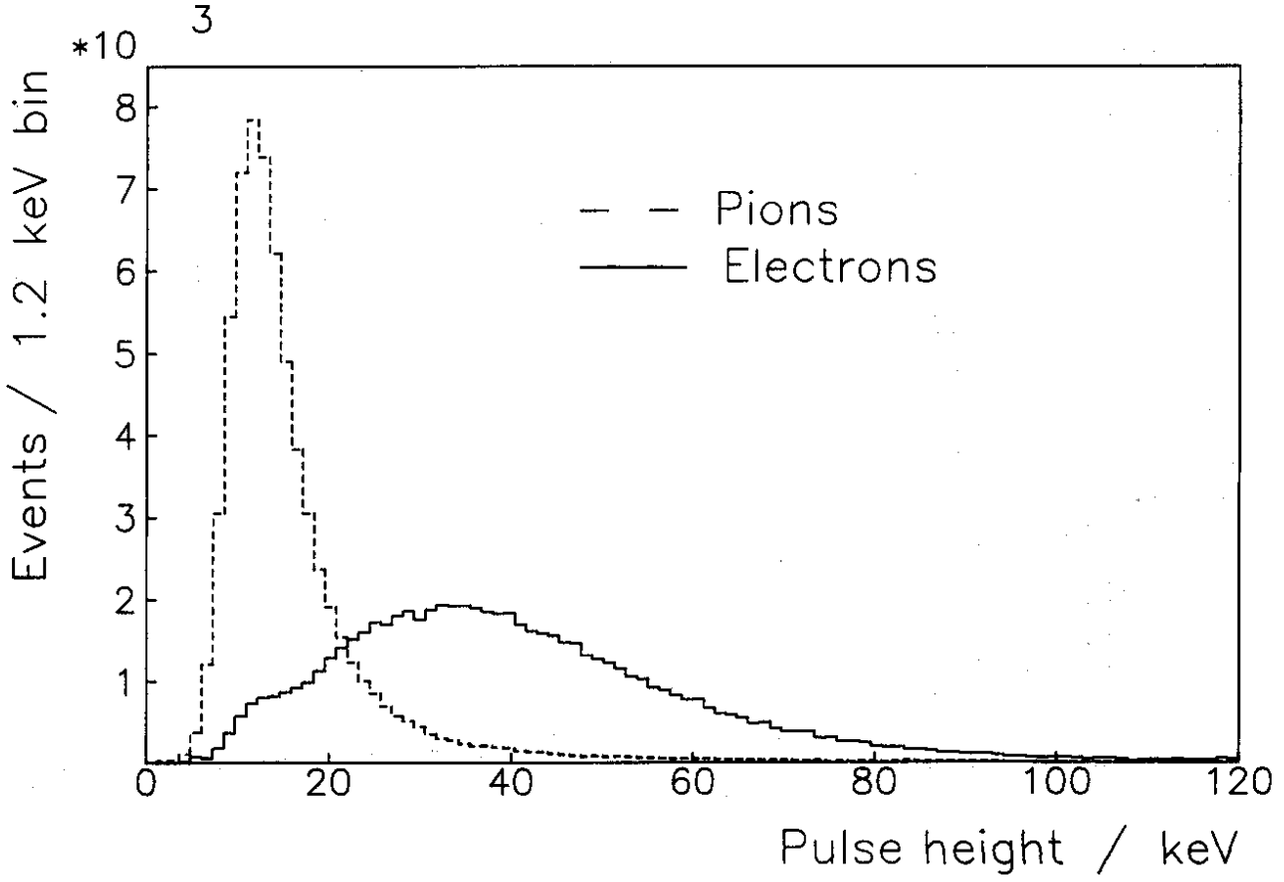
*10 3
Events / 1.2 keV bin
8
7
6
5
4
3
2
1
Pions
Electrons
0
20
40
60
80
100
120
Pulse height / keV

Fig. 10

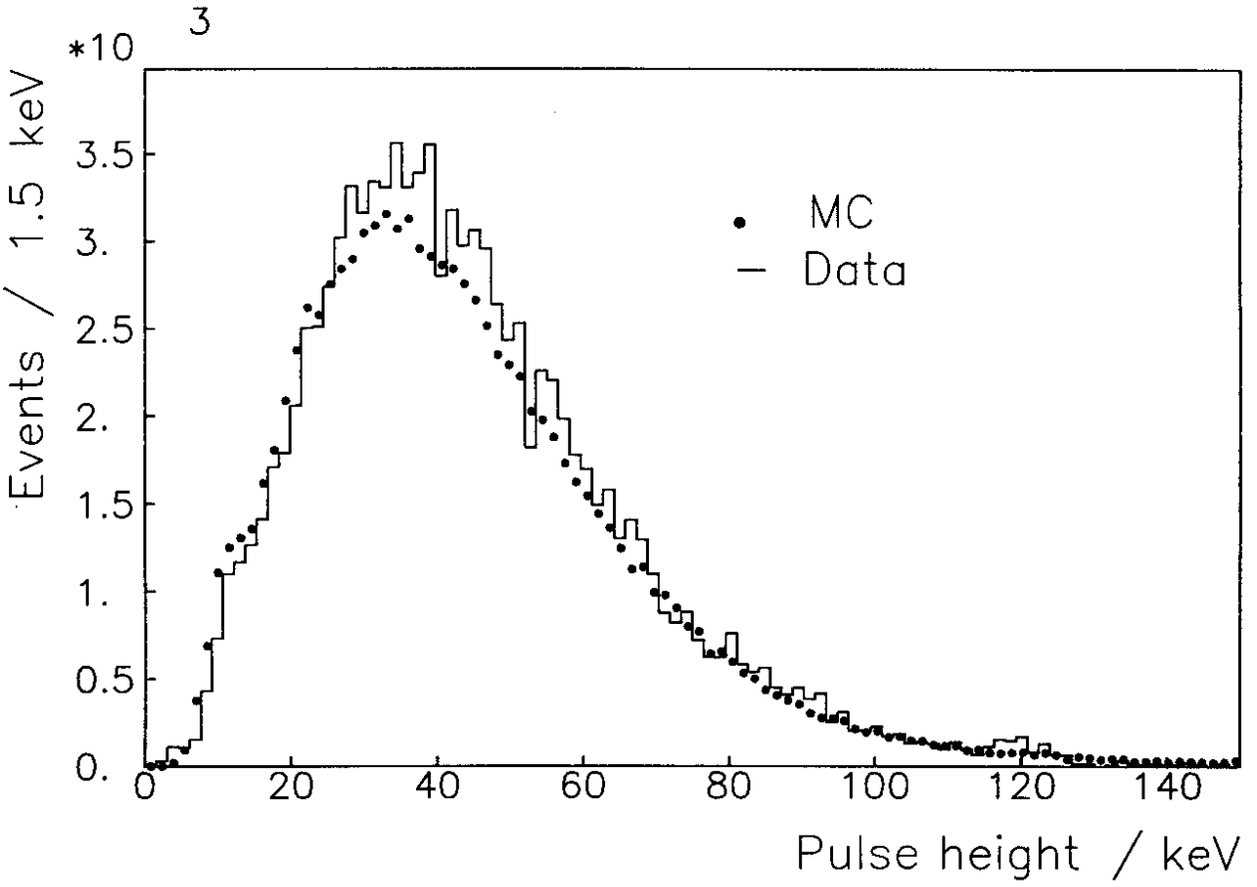
*10 3
Events / 1.5 keV
3.5
3.
2.5
2.
1.5
1.
0.5
0.
0
20
40
60
80
100
120
140
Pulse height / keV
MC
Data

Fig. 11

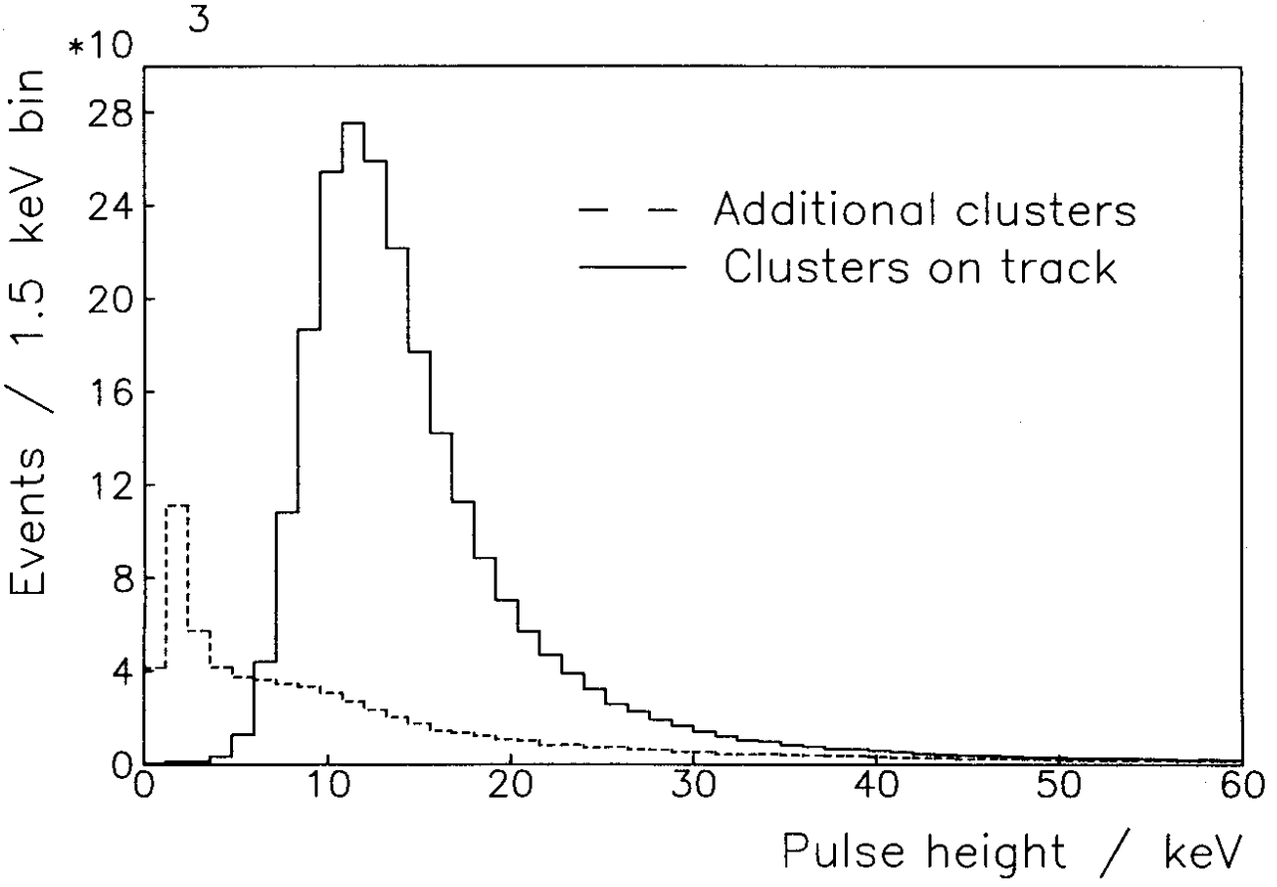
*10 3
Events / 1.5 keV bin
28
24
20
16
12
8
4
0
0
10
20
30
40
50
60
Pulse height / keV
Additional clusters
Clusters on track

Fig. 12

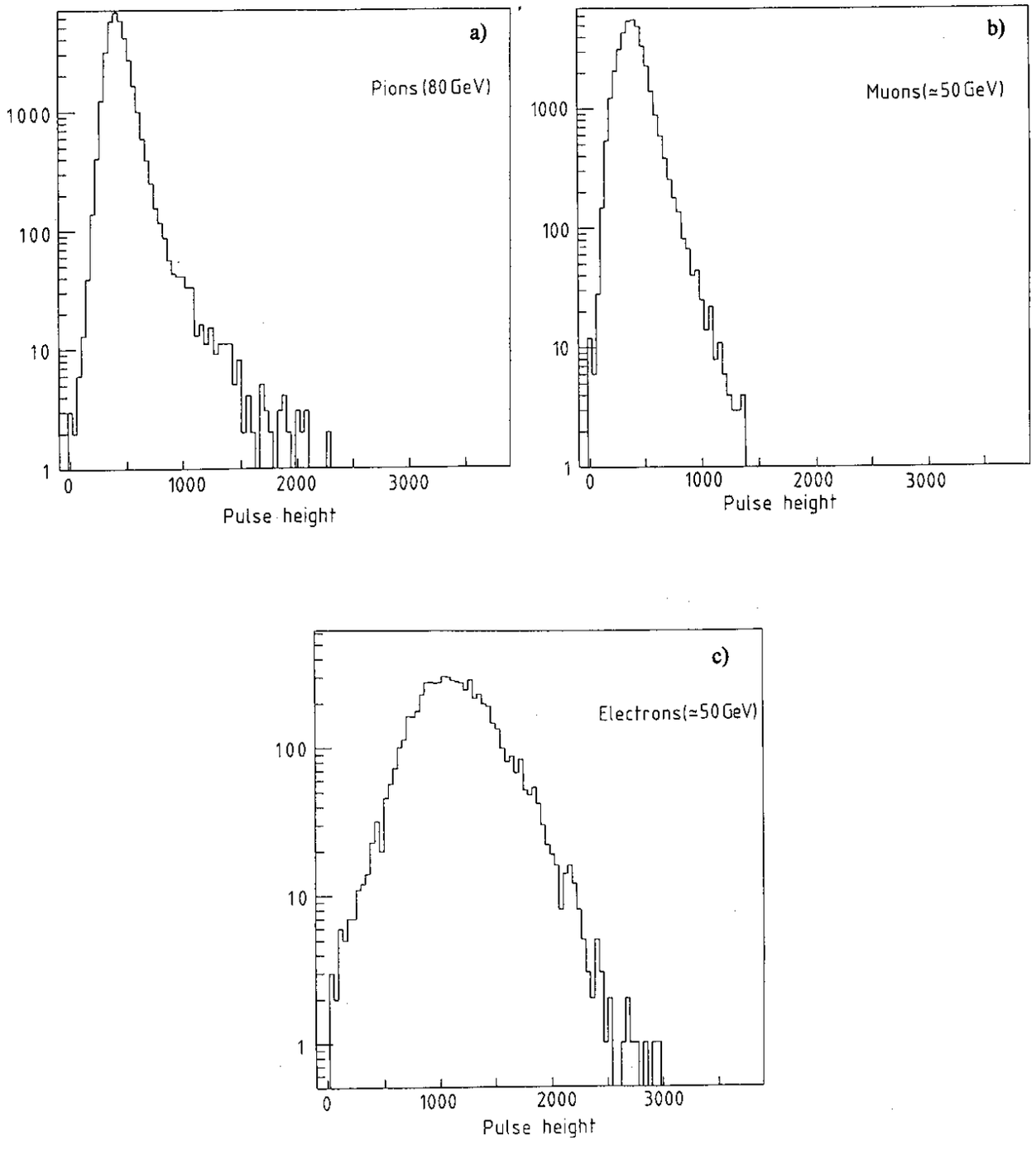
a)
Pions (80 GeV)
1000
100
10
1
0
1000
2000
3000
Pulse height
b)
Muons(≃50 GeV)
1000
100
10
1
0
1000
2000
3000
Pulse height
c)
Electrons(≃50 GeV)
100
10
1
0
1000
2000
3000
Pulse height

Fig. 13

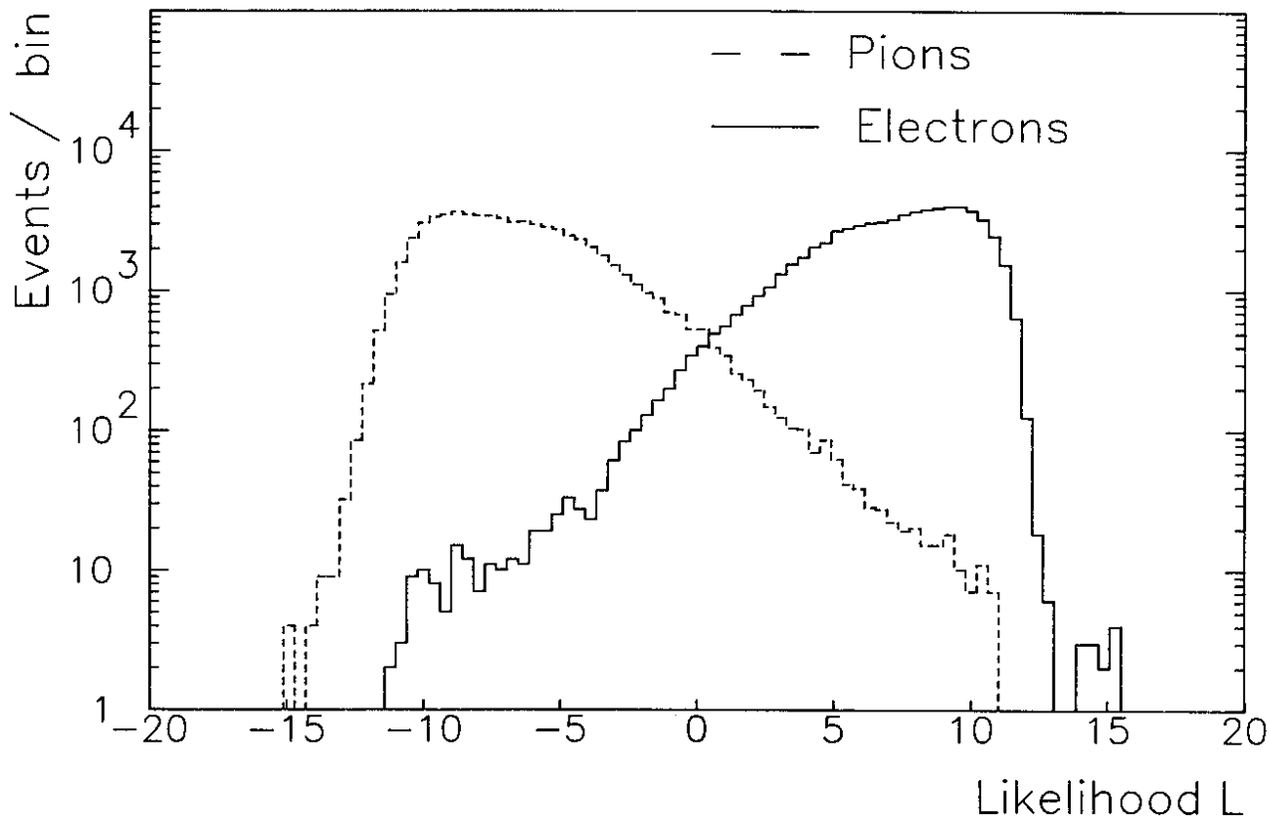
Pions
Electrons
Events / bin
10^4
10^3
10^2
10
1
−20
−15
−10
−5
0
5
10
15
20
Likelihood L

Fig. 14

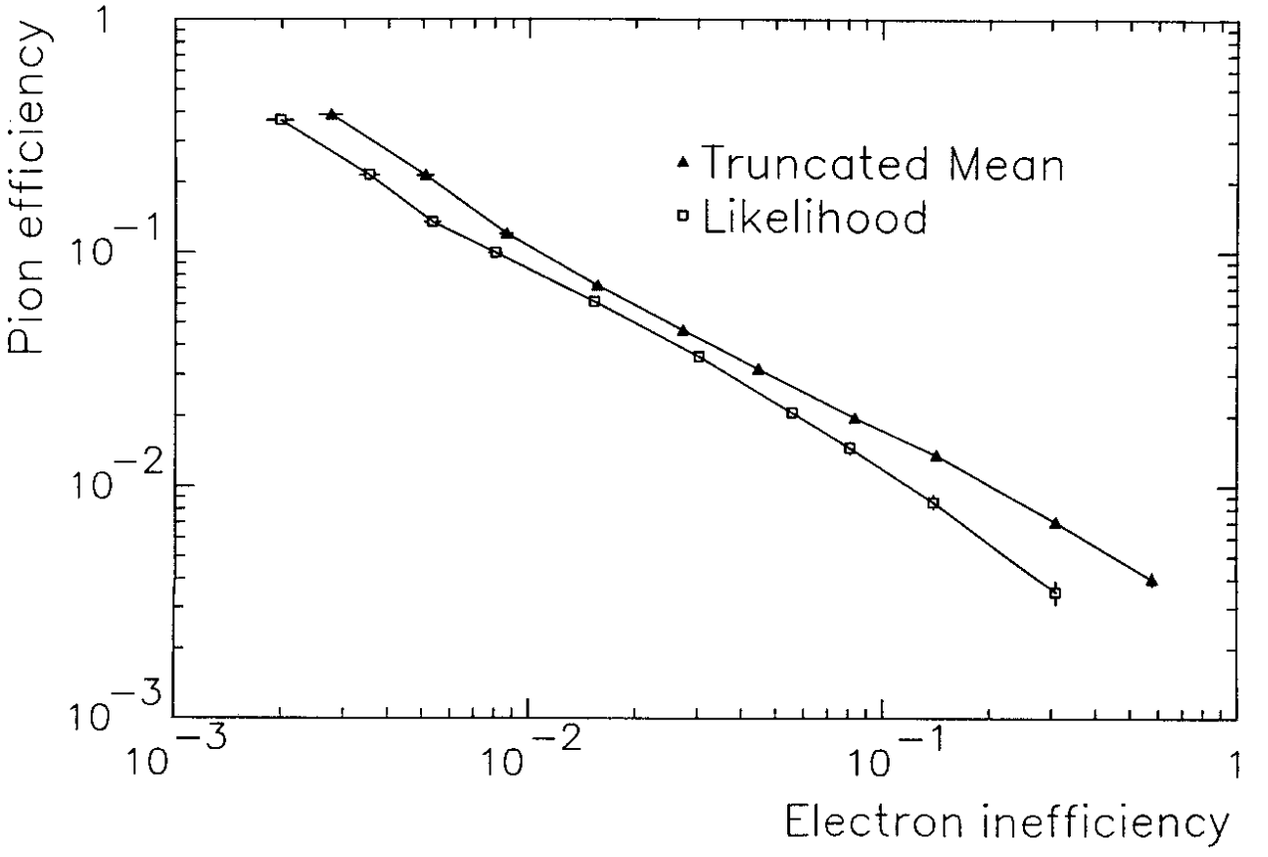
Truncated Mean
Likelihood
Pion efficiency
1
10^{-1}
10^{-2}
10^{-3}
10^{-3}
10^{-2}
10^{-1}
1
Electron inefficiency

Fig. 15